ANNUAL REVIEWS

Annual Review of Analytical Chemistry

Genetically Encoded Sensors for the In Vivo Detection of Neurochemical Dynamics

Yuqing Yang,[1,2,*] Bohan Li,[1,3,*] and Yulong Li[1,2,3,4,5,6]

[1]State Key Laboratory of Membrane Biology, PKU-IDG/McGovern Institute for Brain Research, New Cornerstone Science Laboratory, Beijing, China

[2]School of Life Sciences, Peking University, Beijing, China; email: yulongli@pku.edu.cn

[3]Academy for Advanced Interdisciplinary Studies, Peking–Tsinghua Center for Life Sciences, Peking University, Beijing, China

[4]Chinese Institute for Brain Research, Beijing, China

[5]Institute of Molecular Physiology, Shenzhen Bay Laboratory, Shenzhen, Guangdong, China

[6]National Biomedical Imaging Center, Peking University, Beijing, China

Annu. Rev. Anal. Chem. 2024. 17:15.1–15.26

The *Annual Review of Analytical Chemistry* is online at anchem.annualreviews.org

https://doi.org/10.1146/annurev-anchem-061522-044819

*These authors contributed equally to this article

Keywords

fluorescence microscopy, genetically encoded sensors, neurochemical, in vivo microscopy

Abstract

The ability to measure dynamic changes in neurochemicals with high spatiotemporal resolution is essential for understanding the diverse range of functions mediated by the brain. We review recent advances in genetically encoded sensors for detecting neurochemicals and discuss their in vivo applications. For example, notable progress has been made with respect to sensors for second messengers such as cyclic adenosine monophosphate, enabling in vivo real-time monitoring of these messengers at single-cell and even subcellular resolution. Moreover, the emergence of highly sensitive sensors for neurotransmitters and neuromodulators has greatly accelerated the study of these signaling molecules in a wide variety of behavioral models using an array of powerful imaging techniques. Finally, we discuss the future direction of neurochemical sensors, including their ability to measure neurochemical concentrations and the potential for multiplex imaging.

1. INTRODUCTION

The nervous system relies on neurotransmitters (NTs) and neuromodulators (NMs) to coordinate signaling between cells. In addition, intracellular second messengers such as calcium (Ca^{2+}) and cyclic adenosine monophosphate (cAMP) play an essential role in regulating synaptic transmission and neuronal plasticity. These chemicals work together in an intricately regulated network to drive various physiological processes, including learning and memory, perception, and the sleep–wake cycle. For the purposes of this review, we collectively refer to NTs, NMs, and intracellular messengers as neurochemicals. In addition to hundreds of neurochemicals that function within the nervous system, a wide range of cell types—ranging from neurons to glia—have specific properties and mediate a variety of functions. Therefore, understanding neural circuitry requires a robust set of tools designed to monitor spatial and temporal changes in neurochemicals within a genetically defined population of cells.

Genetically encoded optical sensors have revolutionized the study of neurochemicals by giving researchers the ability to monitor specific neurochemicals, including extracellular NTs and NMs, as well as intracellular second messengers. In this review, we summarize the array of genetically encoded sensors for neurochemicals and discuss their use in vivo in behaving animals for addressing key biological questions. In addition, we discuss future opportunities for developing and applying genetically encoded optical sensors, including their use in (*a*) multiplex imaging and simultaneous recordings and (*b*) quantitative measurements.

2. THE BIOCHEMICAL NATURE OF SIGNALING PATHWAYS AND NEURONAL ACTIVITY AND TRADITIONAL METHODS FOR DETECTION

2.1. Intracellular Second Messengers: Ca^{2+} and cAMP

Throughout several billion years of evolution, cells have adapted to use Ca^{2+} as a crucial signaling species by expressing numerous Ca^{2+}-binding proteins to perform various physiological functions (1). Specifically, neurons employ specialized membrane proteins known as synaptotagmins to sense Ca^{2+} and mediate rapid vesicle fusion, leading to the release of certain types of NTs and NMs (2). Indeed, Ca^{2+} imaging in neurons provides a reliable approximation of neuronal activity, as reviewed extensively by Grienberger & Konnerth (3). Consequently, Ca^{2+} sensors are by far the most widely used in neuroscience. Given the close relationship between increased intracellular Ca^{2+} concentration ($[Ca^{2+}]_i$) and vesicle fusion, $[Ca^{2+}]_i$ has also been used as an indirect measure of vesicle-dependent NT and NM release. This approach is based on the assumption that each type of neuron releases a specific NT or NM; however, single-cell RNA sequencing data suggest that each neuron expresses at least one small-molecule transmitter and one neuropeptide (4), thereby complicating the interpretation of Ca^{2+} imaging in neurons. Furthermore, specific NTs and NMs such as purines (5) and neurolipids (6) can be released via vesicle-independent mechanisms, and the role of Ca^{2+} in these processes remains poorly understood. Thus, the use of Ca^{2+} indicators may not serve as a definitive method for tracking dynamic changes in NT and NM release.

Another key intracellular signaling molecule that regulates the effector function of many NTs and NMs is cAMP, which orchestrates an array of cellular functions in neurons, including morphological properties, neuronal excitability, and synaptic plasticity. By acting on multiple targets—including ion channels, protein kinases, and transcription factors—cAMP can drive a wide range of biochemical processes over timescales ranging from seconds to several days (7). In cells, cAMP is produced by the enzyme adenylyl cyclase, which converts ATP to cAMP; in contrast, the enzyme phosphodiesterase converts cAMP to AMP, thereby reducing cAMP levels. Although

intracellular concentrations of cAMP were previously believed to increase uniformly throughout the cell due to its high diffusion coefficient, emerging evidence suggests that cAMP may accumulate and function locally within cellular "microdomains" (8). In this respect, the development of cAMP sensors may provide new opportunities to study these cAMP microdomains.

2.2. Extracellular Signaling: Chemical Synapses and Neurotransmission

Neurons form complicated networks via chemical synapses, which comprise three structural components: the presynaptic terminal, the synaptic cleft, and the postsynaptic membrane. The presynaptic terminal contains vesicles that are filled with one or more specific NTs and/or NMs, including small molecules and neuropeptides. Note that cell–cell communication via distinct molecules is not unique to neurons but is also used by other cell types, such as glial cells.

Small molecular NTs such as glutamate, γ-aminobutyric acid (GABA), and glycine (9, 10) are classified on the basis of their action on ionotropic (i.e., ion-conducting) receptors, which elicit an electrophysiological response and thereby initiate extremely rapid, spatially restricted synaptic communication [note also that some NTs have corresponding metabotropic G protein–coupled receptors (GPCRs) such as metabolic glutamate receptors and $GABA_B$ receptors, which bind glutamate and GABA, respectively, to drive intracellular signaling via second messengers]. These properties make it possible to measure the release of NTs using highly sensitive electrophysiological recording techniques, which can capture events on a millisecond timescale. Importantly, however, because changes in membrane potential can result from the activity of various NTs, specific receptor antagonists are needed to confirm their molecular specificity (11). Furthermore, electrophysiological recording is technically challenging and is a relatively low-throughput technique, limiting its use primarily to in vitro applications.

In contrast, NMs such as monoamines, neurolipids, and neuropeptides act primarily via metabotropic GPCRs (although some molecules such as serotonin and ATP also have corresponding ionotropic receptors) (12). NMs induce a change in the level of secondary messengers within the recipient cell, thereby changing its electrophysiological properties, metabolism, morphology, and/or transcriptional activity. In contrast to ionotropic signaling, metabotropic signaling has a relatively slow rate and long range due to diffusion, affecting a wider area in the neural circuitry (13, 14). Importantly, not all GPCRs are coupled to ion channels, preventing the use of electrophysiological recordings for detecting the release of some NMs. To overcome this limitation, a range of detection techniques have been developed. Some of them (e.g., Tango assay and cell-based neurotransmitter fluorescent engineered reporters) are reviewed extensively elsewhere (15).

With respect to a suitable detection method, several criteria have been described, including high sensitivity, high molecular specificity, and high spatial and temporal resolution (16). Among the various methods developed to date, optical imaging has shown great potential for meeting most of these criteria, leading to rapid advances in the development of genetically encoded sensors for detecting NTs and NMs (17, 18).

In addition to their distinct modes of action, some NTs and NMs can bind to multiple receptors, with an array of affinities. Thus, even when the same neurochemical is present, its function is determined in part by its concentration. For example, dopamine (DA) receptors are divided into $G\alpha_{s/olf}$-coupled D1-like receptors and $G\alpha_{i/o}$-coupled D2-like receptors. Pharmacologically, D1-like receptors have an affinity 10- to 100-fold lower than that of D2-like receptors (19). In addition, two main types of medium spiny neurons in the striatum express either D1 or D2 receptors, with minimal overlap (20). These findings suggest that the effects of D1 versus D2 receptor signaling will vary depending on extracellular DA concentration (21, 22). Moreover, abnormal levels of NTs and/or NMs are associated with numerous neurological disorders, as reviewed by Carhart-Harris

& Nutt (23). Thus, our ability to correlate NT/NM levels with physiological and/or pathological conditions requires tools that can provide information regarding absolute concentration. Although existing optical techniques may not completely meet the technical requirements needed for accurate quantification, several strategies may help overcome this limitation, a topic we address in the following sections.

3. PHOTOCHEMISTRY AND THE STRUCTURAL BASIS OF GENETICALLY ENCODED SENSORS

The green fluorescent protein (GFP) was discovered in the early 1960s (24), and Chalfie et al. (25) showed nearly three decades ago that GFP can be heterologously expressed in both prokaryotic and eukaryotic cells. These breakthroughs paved the way for the subsequent development and application of various genetically encoded optical tags and sensors for studying biological processes. Compared with other methods, genetically encoded sensors have several unique advantages. For example, they can be expressed in specific cell types, thus providing high cellular specificity. In addition, these sensors are compatible with long-term imaging for days—or even months—when expressed in living cells and animal models (26). These properties make genetically encoded sensors well suited for use in in vivo preparations.

As a general principle of photochemistry, fluorescence occurs when photon-excited molecules decay back to their ground state and emit detectable photons (**Figure 1*a***). The brightness of a fluorophore is determined primarily by two parameters, namely the extinction coefficient and quantum yield. The extinction coefficient describes the fluorophore's efficiency at absorbing excitation light, while the quantum yield is the fluorophore's ability to produce photons and is defined as the ratio of emitted photons to absorbed photons. Both parameters are intrinsic to the fluorophore's chemical composition and can be affected by the microenvironment. In addition to fluorescence intensity, a fluorophore is characterized by its fluorescence lifetime, typically defined as the time in which an excited molecule stays in the excited state. For a single fluorescent protein (FP), the fluorescence lifetime is proportional to the quantum yield. The fluorescence lifetime can be measured using fluorescence lifetime imaging microscopy (FLIM) (27, 28) and is generally not affected by intensity-related factors, thus circumventing the difficulties associated with intensiometric imaging and drawing increasing interest (29–33).

A genetically encoded sensor typically has two components. The first is a sensing module that binds the ligand of interest, and the second is the reporter module, which is usually based on either Förster resonance energy transfer (FRET) or a conformation-sensitive change in a single FP such as GFP. Furthermore, on the basis of readout, these sensors can be further classified as either intensity-based sensors, which provide an intensiometric or ratiometric readout, or FLIM-based sensors, which provide fluorescence lifetime as the readout (**Figure 1*b***). More specifically, in most circularly permuted (cp)GFP-based sensors, the predominant factor contributing to the change in fluorescence intensity is a change in the extinction coefficient, while the change in quantum yield is typically not significant. Consequently, such sensors are suitable only for intensiometric measurements, not lifetime measurements. Therefore, the development of novel FLIM-based sensors requires ways to regulate the sensors' quantum yield (31).

FRET-based sensors are generally easier to develop and can theoretically be used to quantify ligand concentration using the emission ratio or FLIM-FRET. In addition, expressing both the donor and acceptor proteins in a single expression construct helps reduce sensor concentration–based effects. In contrast, several factors can limit the ability to accurately quantify the signal, including wavelength-dependent scattering, differing protein maturation rates between the donor and acceptor, and differences in the emission ratio when using different detection tools (34).

Moreover, the dynamic range of FRET-based sensors is typically rather limited and is determined primarily by the physical distance between the donor and acceptor. Finally, most FRET-based sensors have two emission wavelengths, limiting their application in multiplex imaging.

Compared with FRET-based sensors, single-FP-based sensors are more challenging to engineer, but they have recently become more popular because of several key advantages. First, single-FP-based sensors can achieve a higher dynamic range and provide an intensiometric signal, making them more suitable for use in in vivo applications. Second, their relatively small size makes single-FP-based sensors easier to deliver in in vivo preparations. Moreover, they typically occupy

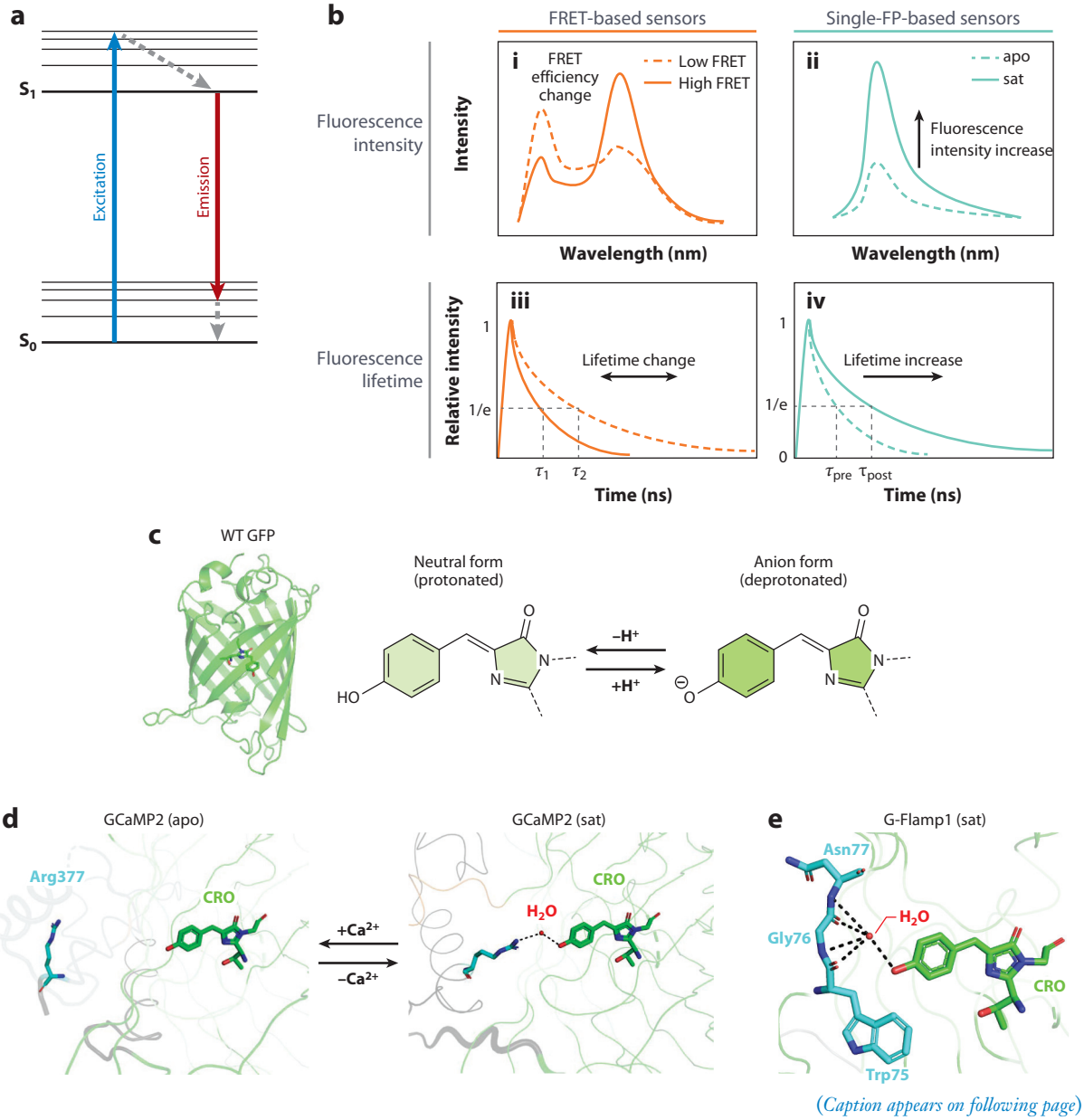

(Caption appears on following page)

Figure 1 (*Figure appears on preceding page*)

Types and structural basis of genetically encoded sensors. (*a*) Jablonski diagram illustrating the principle of fluorescent indicators. S_0 and S_1 represent the ground and excited states, respectively. Excitation light shifts the fluorophore to the excited state, and emission light of a different wavelength is released when the fluorophore decays back to the ground state. (*b*) Overview of the four general types of genetically encoded fluorescent sensors, categorized according to their fluorescence module and signal readout. (*i*) With a FRET-based ratiometric sensor, FRET efficiency is altered upon ligand binding, inducing a change in the sensor's spectrum and emission ratio. (*ii*) With a single-FP-based intensiometric sensor, fluorescence intensity generally increases upon ligand binding; in some cases, ligand binding induces a decrease in intensity (i.e., inverse sensors). Apo refers to the ligand-free state, and sat refers to the ligand-saturated state. (*iii*) Normalized fluorescence lifetime decay curve with the FRET donor in the low-FRET or high-FRET state. The lifetime of the donor FP decreases when FRET occurs, thereby reporting the sensor state. (*iv*) Normalized fluorescence lifetime decay curve with a single-FP-based sensor. The difference in fluorescence lifetime corresponds to different sensor states. (*c*) Crystal structure (PDB ID: 1EMA) of WT GFP, highlighting the chemical composition of the chromophore. The GFP chromophore is constantly shifting between the neutral (protonated) phenol state and ionized (deprotonated) phenolate state. The deprotonated state is typically brighter in fluorescence and is therefore the main contributor to the sensor's signal. (*d*) Structures of the GCaMP2 sensor in (*left*) the Ca^{2+}-free state (PDB ID: 3EKJ) and (*right*) the Ca^{2+}-bound state (PDB ID: 3EVR). In the Ca^{2+}-bound state, the Arg-377 residue is close to the chromophore, allowing the guanidinium side chain to stabilize the protonated form of the chromophore via a water bridge interaction. (*e*) Structure of the G-Flamp1 sensor, highlighting the water bridge between the linker and the chromophore (PDB ID: 6M63). Abbreviations: Arg, arginine; Asn, asparagine; CRO, chromophore; FP, fluorescent protein; FRET, Förster resonance energy transfer; GFP, green fluorescent protein; Gly, glycine; PDB ID, Protein Data Bank identifier; Trp, tryptophan; WT, wild-type.

a single emission wavelength band and are therefore more amenable for use in multiplex imaging. Together, these advantages outweigh their lack of an ability to accurately quantify the signal, and many single-FP-based sensors have been developed.

To create a sensor in which the FP's fluorescence changes based on the local environment, the FP's chromophore must be exposed. This is commonly achieved by circularly permuting the FP—or, in some cases, by splitting the FP—and then linking the FP to the sensing module. The conformational change in the sensing module induced by ligand binding is then transduced to the cpFP, changing the microenvironment around the exposed fluorophore, and causing a measurable, reversible change in fluorescence.

Many single-FP-based sensors have been developed to date and their structural study has helped elucidate how sensors respond to ligand binding. The first mechanistic insights into how single-FP-based sensors respond to ligand binding came from the structure of GCaMP2, a Ca^{2+} sensor based on cpGFP and the calmodulin (CaM)–M13 peptide complex (35, 36). In wild-type GFP, three consecutive residues (threonine–tyrosine–glycine) form the chromophore and are protected from solvent by surrounding β-sheets. The fluorophore in wild-type GFP exists in two forms depending on the protonation state of the phenol group in the tyrosine residue (37). In the neutral (i.e., protonated) state, the chromophore has an absorption peak at 395 nm, while the ionized (i.e., deprotonated) form has an absorption peak at 475 nm (**Figure 1*c***). Of these two forms, the ionized form contributes to the majority of the chromophore's fluorescence. A structural analysis of both the Ca^{2+}-free and Ca^{2+}-bound forms of GCaMP2 revealed that Arg-377 in the CaM domain plays a key role in determining the sensor's fluorescence response (35). In the Ca^{+}-free state, Arg-377 is located relatively far from—and therefore does not interact directly with—the chromophore, causing the chromophore to reside predominantly in the neutral state. Ca^{2+} binding induces a conformational change that moves the Arg-377 residue closer to the chromophore, allowing a water bridge to form. As a result, the fluorophore is stabilized in the ionized state and the fluorescence increases. This change in the chromophore's protonation state, combined with changes in the fluorophore's extinction coefficient and quantum yield, provides the mechanism by which GCaMP2 responds to an increase in Ca^{2+} concentration (**Figure 1*d***).

The mechanism by which fluorescence changes in response to ligand binding may vary widely from sensor to sensor, as suggested by structural studies of a large variety of sensors (38–42). For example, in the cAMP-bound state, the cAMP sensor G-Flamp1 (42), which is based on

cpGFP and a bacterial cyclic nucleotide–binding domain, has a unique N-terminal linker structure that contains a highly twisted β-strand and is in close proximity to the chromophore in GFP. A closer examination of the structure revealed that the Trp-75 residue in the N-terminal linker helps stabilize the chromophore, both by forming a water bridge and by protecting the chromophore from solvent quenching (**Figure 1*e***). The apparent significance of the Trp-75 residue was further supported by molecular dynamics simulations and saturation mutagenesis (42).

In summary, the change in a sensor's fluorescence can occur via the interaction between the chromophore and adjacent residues in a broad range of sensor domains. Mechanistic insights based on structural studies will likely facilitate the development of high-performance sensors. Such high-performance sensors are expected to have improved optical properties and are better suited for use in biological applications.

4. IMAGING NEUROCHEMICALS USING GENETICALLY ENCODED SENSORS

4.1. Genetically Encoded Ca^{2+} Sensors

Given the important role of $[Ca^{2+}]_i$ in a wide variety of physiological processes, it is not surprising that a variety of both chemical Ca^{2+} sensors and genetically encoded Ca^{2+} indicators (GECIs) have been developed, the earliest of which were introduced in the 1960s (43–45). However, the first truly groundbreaking advance in Ca^{2+} dyes can be attributed to Tsien and colleagues (46, 47). Prior to the wide application of GECIs, Ca^{2+} dyes had already been used to detect Ca^{2+} changes both in vitro and ex vivo. Although commercially available Ca^{2+} dyes are highly sensitive and have been used quite extensively, as small molecules they cannot selectively label specific cell types and sometimes require highly skilled microinjection techniques for in vivo applications. In contrast, genetically encoded indicators offer a more straightforward means to be readily expressed in living animals. Using cell type–specific promoters and/or recombinase-based approaches, these sensors can achieve specificity in genetically defined cell populations. Moreover, the discovery and subsequent optimization of GFP and similar FPs have opened a new world of possibilities in this field.

In 1997, the Tsien group (47) developed the first GECI, a fluorescent Ca^{2+} indicator in which the cyan fluorescent protein–yellow fluorescent protein (CFP-YFP) FRET pair was flanked by CaM and the CaM-binding peptide (CBP) M13. The rationale for this sensor was based on the reversible "wrapping" of CaM and M13 upon binding Ca^{2+} ions, which increased FRET efficiency between CFP and YFP (**Figure 2*a***). Further advances led to the development of FRET-based Ca^{2+} sensors with a higher dynamic range and improved kinetics; these new sensors were then successfully expressed in several animal models, including *Drosophila* and mice (48, 49).

The design of single-FP-based Ca^{2+} indicators is similar in some respects to that of FRET-based sensors. With a single-FP-based Ca^{2+} indicator, a single fluorophore is inserted into the CaM-CBP domain (50, 51). This design was based on the discovery of cpFPs by Baird et al. (52) in the late 1990s (**Figure 2*a***). Over the course of more than two decades, single-FP-based sensors have been optimized, resulting in sensors that often have superior dynamics compared with those of FRET-based sensors.

Among these single-FP-based Ca^{2+} sensors, the GCaMP series stands out. As a result of extensive research and development, GCaMP sensors are now considered state-of-the-art tools for imaging Ca^{2+} dynamics in vivo (53). For example, GCaMP6f can respond to a single action potential–induced Ca^{2+} increase within 50 ms, and the decay half-life is 142 ms. The affinity of GCaMP6f is 375 nM, approximately three- to sevenfold lower than the resting level of $[Ca^{2+}]_i$

(50–100 nM). The suitable affinity and fast kinetics allow the sensor to readily catch up with the increase of $[Ca^{2+}]_i$ during action potential and other intracellular Ca^{2+} mobilization processes. The dynamic ranges of purified protein of GCaMP6 sensors are around 38- to 63-fold, superior to those of the previous GCaMP3 (12.3-fold) and GCaMP5 (17.4–32.7-fold) versions. Indeed, the outstanding performance of these sensors has led to their widespread use in virtually all model

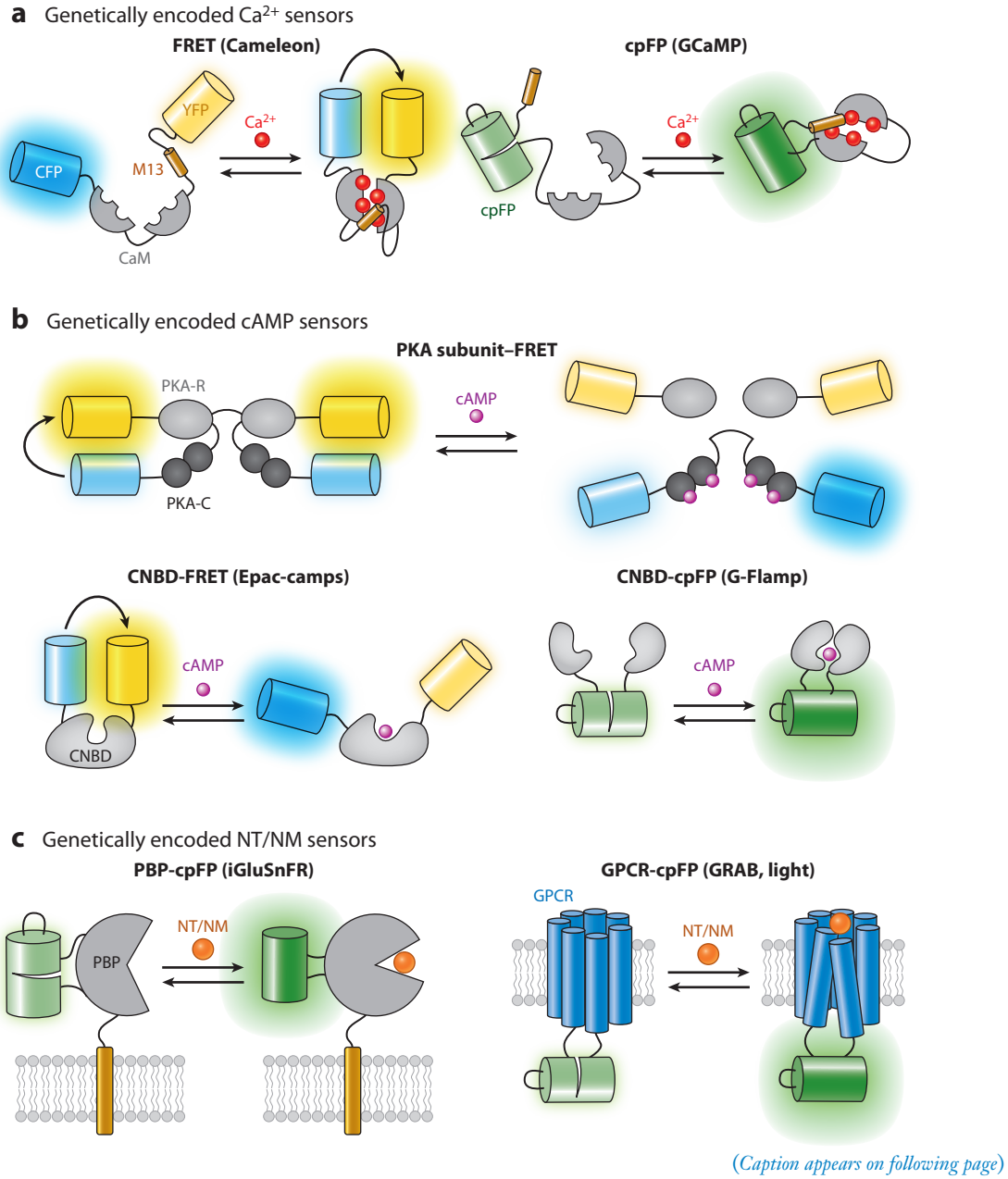

(*Caption appears on following page*)

Figure 2 (*Figure appears on preceding page*)

Genetically encoded indicators for detecting neurochemicals. (*a*) Schematic depiction of GECIs. Two types of GECIs have been developed. (*Left*) FRET-based GECIs are created by inserting the CaM domain and a CaM-binding peptide (e.g., M13) into FRET pair FPs such as the CFP-YFP pair used in Cameleon. (*Right*) In contrast, cpFP-based GECIs are created by inserting a cpFP into M13 and CaM, as shown for the GCaMP series of sensors. Closure of the narrow split in the cpGFP represents the environment of the cpGFP chromophore upon calcium binding. (*b*) Schematic depiction of genetically encoded cAMP indicators. cAMP indicators have been developed according to several principles, including PKA holoenzyme subunits and CNBDs. (*Top row*) A FRET-based sensor using PKA holoenzyme subunits was developed by fusing the FRET donor to the PKA-R (regulatory) subunit and fusing the FRET acceptor to the PKA-C (catalytical) subunit. (*Bottom left*) With FRET-based cAMP indicators that use CNBDs as the single cAMP-binding domain, CFP and YFP are fused to the N-terminal and C-terminal domains of CNBD, and cAMP levels are reported as a change in the FRET ratio. Epac-camps is an example of this sensor type. (*Bottom right*) Finally, similar to cpFP-based Ca^{2+} indicators, cpFP can be inserted into a CNBD to generate an intensiometric cAMP indicators such as G-Flamp1. (*c*) Schematic depiction of genetically encoded NT/NM indicators. Two general categories of NT/NM indicators have been developed on the basis of the ligand-binding protein used (i.e., PBPs or GPCRs). (*Left*) With single-fluorophore indicators that use a PBP, the cpFP is inserted into the PBP's hinge region (e.g., iGluSnFR). (*Right*) With GPCR-based fluorescent indicators, the cpFP is inserted into the receptor's third intracellular loop of the GPCR (e.g., GRAB, Light). Abbreviations: CaM, calmodulin; CNBD, cyclic nucleotide–binding domain; cpFP, circularly permuted FP; FP, fluorescent protein; FRET, Förster resonance energy transfer; GECI, genetically encoded Ca^{2+} indicator; GPCR, G protein–coupled receptor; NM, neuromodulator; NT, neurotransmitter; PBP, periplasmic binding protein; PKA, protein kinase A. In panel *a*, the diagram of FRET-based GECIs is adapted from Reference 47, and the cpFP-based Ca^{2+} sensor image is adapted from Reference 50. In panel *b*, the diagram of the PKA subunit–based cAMP indicators is adapted from Reference 63, the CNBD-based FRET cAMP indicator image is adapted from Reference 150, and the CNBD-based cpFP cAMP indicator image is adapted from Reference 42. In panel *c*, the diagram of PBP-based NT/NM indicators is adapted from Reference 82, and the GPCR-based indicator image is adapted from References 89 and 90.

organisms, and they are highly compatible with a wide range of imaging techniques, including fiber photometry recording, multiphoton imaging, and the recently developed mesoscopic wide-field imaging.

In many respects, GCaMP sensors revolutionized the field of Ca^{2+} imaging, allowing researchers to visualize Ca^{2+} dynamics in living organisms with high precision and high spatiotemporal resolution. Recent advances and the expansion of GFP-based Ca^{2+} indicators have further improved these sensors' response, brightness, and kinetics. For example, replacing enhanced GFP with mNeonGreen (an exceptionally bright FP derived from the cephalochordate *Branchiostoma lanceolatum*) led to the NEMO series of sensors, with wide dynamic ranges and brightness (54). In addition, by screening various CBP domains, investigators have developed jGCaMP8 sensors with faster on and off kinetics (55). The off kinetics of the jGCaMP8f is 37.03 s^{-1}, which is around ten times faster than that of GCaMP6f (3.93 s^{-1}) and more than five times faster than that of jGCaMP7f (7.34 s^{-1}).

Several other series of single-FP-based Ca^{2+} indicators have been developed. Multiplex imaging requires sensors with distinct, nonoverlapping spectra colors, which prompted the development of the GECO and XCaMP series of GECIs, in which the original cpGFP module was replaced with other FPs (56, 57). Highly sensitive red fluorescent Ca^{2+} indicators, such as the jRGECO and jRCaMP series, have also been created (58). These indicators offer clear advantages over green fluorescent indicators, including lower phototoxicity and deeper penetration of light into living tissue. Recently, far-red Ca^{2+} imaging became possible with the introduction of far-red FPs (59, 60) and cp-protein tags with far-red chemical dyes (61), greatly expanding the toolkit of Ca^{2+} indicators. These advances now provide researchers with various options for Ca^{2+} imaging, with improved sensitivity, the ability to perform multiplex imaging, and increased imaging capabilities. For instance, a study by Inoue et al. (57) simultaneously utilized GFP-, blue fluorescent protein–, and red fluorescent protein–based calcium indicators to monitor different cell types in behaving mice. However, the use of blue sensors in in vivo applications is less preferred, because their excitation light (~385 nm) has compromised tissue penetrance and their

emission light (~450 nm) falls within the range of enhanced autofluorescence from biological samples. An alternative approach involves employing far-red sensors, which not only overcome these limitations but also allow for four-color multiplexed imaging.

Another advantage of GECIs is their ability to target specific tissues using cell type–specific promoters and/or transgenic lines. Moreover, through the addition of targeting motifs, these sensors can even be directed to specific subcellular compartments, facilitating the imaging of structures such as the axon, soma, or endoplasmic reticulum so as to provide high versatility and specificity.

4.2. Genetically Encoded cAMP Sensors

Various genetically encoded sensors developed over the past 30 years have contributed considerably to our understanding of cAMP signaling. Genetically encoded cAMP sensors have been developed using various downstream effector protein domains as the sensing module. The first such sensor, FlCRhR [fluorescein-labeled protein kinase A (PKA) catalytic (PKA-C) subunit and rhodamine-labeled regulatory (PKA-R) subunit (62)], is based on dissociation of the PKA holoenzyme and consists of two fluorescent modules fused to the PKA-R and PKA-C subunits. When cAMP binds to the PKA-R subunit, the PKA-C subunit dissociates, inducing a FRET signal. However, FlCRhR is not fully genetically encoded and requires microinjection into the organism together with tagged rhodamine and fluorescein. Subsequent versions of this sensor based on PKA holoenzyme dissociation use FPs instead of fluorescent dyes and are fully genetically encoded. Subsequent optimization included the use of higher-efficiency FRET pairs and fine-tuned the linker domains (63–66) (**Figure 2*b***).

Single-polypeptide cAMP sensors exploit the conformational change induced by cAMP binding to its effector proteins such as PKA, Epac (exchange protein directly activated by cAMP) (67–69), and cAMP-dependent ion channels (70). Moreover, FRET efficiency can be optimized by fusing FPs to the N-terminal and C-terminal domains of these effector proteins, or truncated versions containing the cAMP-binding domain. For example, considerable effort has led to optimized Epac-based FRET cAMP sensors with a high FRET ratio (**Figure 2*b***), including a series of FLIM-FRET-based cAMP sensors (71). Moreover, the use of cpFPs to develop a sensor led to green fluorescent cAMP sensors based on cpGFP (42, 72) and its red-shifted variants (73, 74), offering a significant change in fluorescence and wide versatility for in vivo applications. Despite their relatively brief history, single-FP-based cAMP sensors have made significant strides in the past decade, and their compact size and potential for producing a larger fluorescence response will likely result in even further advances in the field (**Figure 2*b***).

Note that a wide array of genetically encoded sensors have been developed to monitor the activity of PKA, a major downstream effector of cAMP. We do not cover PKA sensors in this review because PKA is generally not considered a neurochemical; however, PKA sensors have been reviewed thoroughly by several other groups (32, 75, 76).

4.3. Genetically Encoded Sensors for Extracellular Neurochemicals

The mammalian brain uses more than 100 known NTs and NMs, each of which plays an important role in complex processes such as signaling transmission (13). In addition, drugs that target NT and/or NM receptors—or NT and/or NM metabolic enzymes—have shown promise in treating various neurological conditions. For example, decreased serotonin levels are widely believed to play a central role in depression, and the selective serotonin reuptake inhibitor fluoxetine (Prozac) acts as an effective antidepressant by increasing serotonin levels in the synaptic cleft (77). Over the

past two decades, numerous sensors for NTs and NMs have been developed, allowing researchers to perform in vivo imaging with high spatiotemporal resolution.

Depending on the sensing module, NT and NM sensors can be categorized into two major groups, namely sensors based on a periplasmic binding protein (PBP) and sensors based on a GPCR (see **Supplemental Table 1**). PBPs are a group of proteins typically consisting of two large lobes that surround the bound ligand, resembling a Venus flytrap (78). These proteins undergo a large conformational change upon ligand binding, making them a promising scaffold for engineering biosensors.

The strategy for developing the first PBP-based NT sensors FLIPE (79) and GluSnFR (80, 81) involved inserting the glutamate-binding protein into CFP and YFP. Because the PBP is displayed on the outer surface of the cell membrane, any changes in FRET efficiency reflect a change in extracellular glutamate concentration. Inspired by cpGFP-based GECIs, investigators then developed a series of single-FP-based sensors using PBPs; the first, and perhaps the most widely used, are the iGluSnFR series (82–84) (**Figure 2*c***). Further engineering of iGluSnFR led to next-generation iGluSnFR3 versions with faster kinetics (approximately twice as fast compared with the previous-generation SF-iGluSnFR) and higher sensitivity under two-photon excitation (~20-fold response improvement compared with SF-iGluSnFR) (see **Supplemental Table 1**). The success of iGluSnFR paved the way for the development of a broad range of sensors for detecting NTs and NMs, including—but by no means limited to—acetylcholine (ACh) (85), serotonin (86), and GABA (87).

Although the large ligand-induced conformational change in PBPs leads to a large dynamic change, not every NT and NM has a corresponding PBP, particularly in the case of neuropeptides. Indeed, most PBP-based sensors developed to date have been designed to detect small molecules and usually require considerable effort to optimize their affinity and molecular specificity.

The introduction of GPCR-based biosensors started a new era in the detection of NTs and NMs. Unlike PBPs, GPCRs serve as the body's own sensors for NTs and NMs. Moreover, as transmembrane proteins, most GPCRs function at the cell surface, reducing the need to engineer the sensor to target the plasma membrane. These advantages make GPCRs attractive scaffolds for building genetically encoded biosensors. Several decades of extensive study have revealed that most GPCRs contain a highly conserved conformational change in the TM5 and TM6 domains upon activation (88). By replacing the receptor's third intracellular loop between TM5 and TM6 with cpFP modules, researchers developed two major families of GPCR-based sensors, namely the GRAB (89) and Light (90) sensors (**Figure 2*c***). GPCR-based sensors have recently been developed for an array of NTs and NMs, including monoamines (91–94), purines (95, 96), neurolipids (97), and neuropeptides (98, 99). Because these sensors are derived from their respective GPCRs, they have a good affinity for detecting changes in endogenous NTs and NMs. Moreover, by systematically modifying the linker region, the cpFP module, and/or the GPCR itself, these optimized sensors can have remarkably high sensitivity, making them ideal for monitoring NT/NM release in vivo (see **Supplemental Table 1**).

Note, however, that certain GPCRs have a promiscuous response to structurally similar chemicals. For example, several opioid receptors can respond to a wide range of endogenous peptide ligands. The DA receptor D1R also shows modest affinity toward norepinephrine (NE). The native oxytocin (OT) receptor can be activated by arginine vasopressin, which is evolutionarily homologous to OT. Sensors developed with such GPCR backbones also display similar ligand specificity. In order to distinguish between different endogenous ligands, extensive molecular engineering in the GPCR domain of the sensor is often required. By mutating amino acids that interact with the ligands in the ligand binding pocket, one can tune the sensors' selectivity for higher specificity to distinguish between different endogenous ligands.

5. DETECTING NEUROCHEMICALS IN VIVO

5.1. Approaches for Detecting Neurochemicals In Vivo with Fluorescent Sensors

Two primary methods have been employed to capture fluorescence signals from biosensors in living animals: fiber photometry and microscopy. Fiber photometry enables the collection of an integrated fluorescence signal through an optical fiber from a targeted brain region; thus, it lacks spatial resolution. The surgical and imaging procedures associated with fiber photometry are user-friendly, and this technique can easily be applied to freely moving animals. This technique not only allows for deep tissue imaging but also enables simultaneous multichannel recording from different brain regions (100). In contrast, one-photon and multiphoton microscopy have been utilized to visualize neurochemical dynamics with spatial resolution. Prior to imaging, the cortical surface needs to be exposed through relatively complex surgical procedures, such as thinning the skull or replacing it with a cover glass (101, 102). Additionally, the implantation of a gradient index lens is necessary to access deep brain regions (103). While traditional microscopies are typically used on head-fixed animals, the recent development of miniature microscopes has enabled imaging in freely moving animals (104, 105). In summary, these two methods complement each other, and researchers should select the appropriate technique according to their specific scientific inquiry.

5.2. Recent Advances in Imaging cAMP Levels In Vivo

Studying the important role of cAMP in key processes requires the use of cAMP sensors in both physiological and pathological conditions. In the past dozen years, cAMP sensors have been used in cultured cells and other in vitro applications (32). However, compared with in vitro imaging, in vivo applications require sensors with higher brightness, a larger dynamic range, a sufficiently high signal-to-noise ratio (SNR), and an affinity for cAMP that is compatible with endogenous cAMP levels under physiological conditions. Considerable efforts by sensor developers and input from their end users have given rise to cAMP sensors suitable for in vivo imaging. In this section, we summarize recent advances in the use of genetically encoded cAMP sensors to monitor cAMP in living animals during biologically relevant behaviors.

First, the cpGFP-based sensor G-Flamp1 has been expressed in live zebrafish, *Drosophila*, and mice (42). When G-Flamp1 was coexpressed with the red Ca^{2+} sensor jRGECO1a to simultaneously monitor cAMP and Ca^{2+}, respectively, using two-photon in vivo microscopy in the mouse M1 cortex during forced running, differences between cAMP and Ca^{2+} dynamics were observed, suggesting that these two signals may be regulated via relatively independent processes (**Figure 3*a***). G-Flamp1 is also compatible with in vivo fiber photometry and has been used in mice to report changes in cAMP levels during learning and memory in the nucleus accumbens in the ventral striatum. In addition, the FRET-based sensor cAMPFIRE (71) was combined with FRET-FLIM and two-photon microscopy for long-term imaging of cAMP levels in the mouse cortex for more than a month. The authors of this study (71) also used cAMPFIRE to monitor cell-specific changes in cAMP during forced running and identified three distinct groups of L2/3 pyramidal neurons that respond differently during running; specifically, one group of neurons had a positive response, another group had a negative response, and the third group had a small response (**Figure 3*b***). Although further advances in sensor development are needed, these studies clearly illustrate the potential of using existing cAMP sensors in living animals during behavioral activities and in other biological contexts to better understand the functional role of cAMP and its interactions with other neurochemicals in the central nervous system.

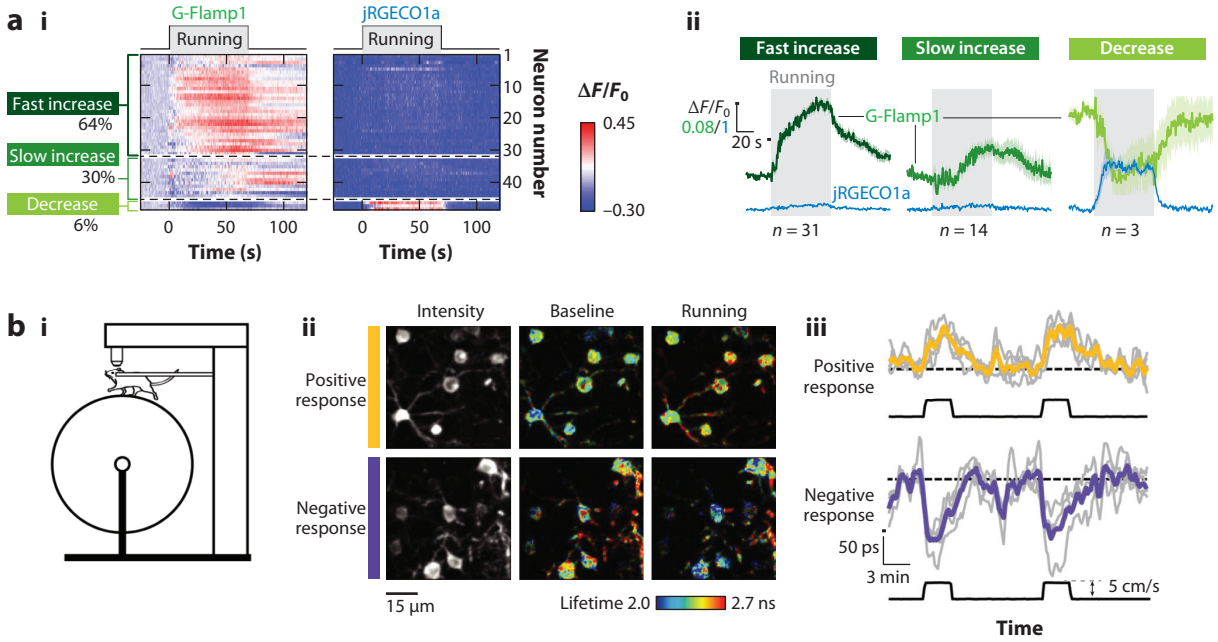

(Caption appears on following page)

Figure 3 (*Figure appears on preceding page*)

In vivo applications of genetically encoded neurochemical sensors. (*a*) Two-photon dual-color in vivo imaging of cAMP and Ca^{2+} levels in M1 cortical neurons in mice during forced running. The neurons can be classified into three groups on the basis of their intrinsically heterogeneous cAMP and Ca^{2+} signals. (*b*) Two-photon FRET-FLIM imaging of cAMP in layer 2/3 cells during forced running. (*i*) Schematic of the enforced running behavioral paradigm. A head-fixed mouse is put on a motorized treadmill. (*ii*) Representative image of fluorescence intensity and lifetime of a cAMP sensor of individual neurons during forced running. (*iii*) Traces of a cAMP sensor from positive- and negative-response neurons during forced running. (*c*) Simultaneous recording of OT in the PFC, PVN, and VTA during various mating behaviors. (*i*) Schematic of the fiber photometry setup for recording OT signals. The optical fibers record signals in three different regions expressing the OT sensor. The mating process consists of three stages: sniffing, intromission, and ejaculation. (*ii*) The fiber photometry signals of the OT sensor in three brain regions during mating. (*d*) Long-term simultaneous recording of histamine in mouse PFC and POA during the sleep–wake cycle. (*i*) Schematic of the fiber photometry setup for recording histamine dynamics in the PFC and POA, which receive histaminergic projection from the TMN. (*ii*) Representative traces of EEG, EMG, and histamine sensor signal in the PFC and POA during the sleep–wake cycle. The wake state is shown in blue, REM sleep is in pink, and NREM sleep is unshaded. Overall, the changes in histamine are similar between these two brain regions, but the histamine signal in the POA has relatively fast on kinetics during the sleep-to-wake transition. (*iii*) Averaged traces of histamine dynamics in the PFC and POA during the sleep state transition. (*e*) Simultaneous electrophysiological recording and iGluSnFR3 imaging of a single cortical neuron, with iGluSnFR3 reporting glutamate release from individual synaptic boutons. (*i*) Experimental schematic for simultaneous two-photon axonal imaging and cell-attached recording in vivo. (*ii*) A *z*-projection of iGluSnFR3-labeled neuron in mouse V1, with an axon outlined in yellow. (*iii*) Magnified image of a neuron axon expressing iGluSnFR3. Three neighboring boutons are labeled. (*iv*) The yellow traces represent the iGluSnFR3 signal from three neighboring boutons, asterisks indicate putative synaptic release failures, and the black trace represents the membrane potential of the same neuron. Abbreviations: EEG, electroencephalogram; EMG, electromyography; FRET-FLIM: Förster resonance energy transfer–fluorescence lifetime imaging microscopy; HA, histamine; LED, light-emitting diode; LT, lifetime; NREM, non-REM; OT, oxytocin; PFC, prefrontal cortex; PMT, photomultiplier tube; POA, preoptic area; PVN, paraventricular nucleus of the hypothalamus; REM, rapid eye movement; TMN, tuberomammillary nucleus; VTA, ventral tegmental area. Panel *a* adapted with permission from Reference 42; copyright 2022 Springer Nature. Panel *b* adapted with permission from Reference 71; copyright 2022 Springer Nature. Panel *c* adapted with permission from Reference 99; copyright 2023 Springer Nature. Panel *d* adapted with permission from Reference 93; copyright 2021 Elsevier. Panel *e* adapted from Reference 84 (CC BY 4.0).

5.3. Using Neurotransmitter and Neuromodulator Sensors to Gain Insights into In Vivo Biological Processes

Fully understanding how the brain works requires the ability to observe neural activity in vivo with high spatiotemporal resolution and minimal experimental interference. Thus, our growing toolbox of neurochemical sensors now allows researchers to tackle many key questions and design experiments with increased flexibility, thereby advancing our understanding of brain function.

The ability to capture dynamic changes in neurochemicals in mice engaged in natural and learned behaviors can increase our understanding of the neural mechanisms that underlie these behaviors. As mentioned above, fiber photometry is an exceptionally good tool for studying neurochemical changes of deep brain regions in freely moving mice. Several studies have used DA sensors to study changes in DA release during both innate and learned behaviors. For example, Dai et al. (106) found sexual dimorphism in dopaminergic signaling in the nucleus accumbens during mating and aggression. In addition, by measuring DA and cAMP signaling in the hypothalamus, Zhang et al. (107) identified a group of specialized dopaminergic neurons that motivate mating behaviors in male mice by activating the cAMP-PKA pathway. The peptide hormone and neuromodulator OT have also been studied using two independently developed sensors called $GRAB_{OT}$ (99) and $MATRIA_{OT}$ (98). $MATRIA_{OT}$ has been used to detect changes in OT under several conditions, including social interactions and acute stress, while $GRAB_{OT}$ has been used to simultaneously record the soma and projection targets during mating behaviors, revealing compartmentalized OT release (**Figure 3*c***).

How neurochemical signaling regulates the sleep–wake cycle is another significant yet open question in neuroscience. Studies have shown that specific brain regions play an essential role in maintaining the sleep–wake cycle (108, 109); however, the specific changes that occur in

various NTs and NMs during transitions between various sleep states—critical for understanding the function of individual neurochemicals—remain largely unexplored. The emergence of neurochemical sensors is now providing researchers the opportunity to tackle these questions. For example, using a newly developed genetically encoded adenosine sensor, Peng et al. (96) simultaneously recorded Ca^{2+} signals and adenosine levels in the mouse basal forebrain; surprisingly, they discovered a neuronal activity–dependent rapid increase in extracellular adenosine levels, even during REM (rapid eye movement) sleep. Dong et al. (93) recently used $GRAB_{HA}$ sensors to identify differences in histamine release between the prefrontal cortex and preoptic area during the sleep–wake cycle in freely moving mice, suggesting possible heterogeneity among histaminergic neurons and/or local regulation of histaminergic terminals in specific brain regions (**Figure 3*d***). Another monoamine that plays an important role in arousal, NE, has also been studied during the sleep–wake cycle using $GRAB_{NE}$ sensors; specifically, fiber photometry recordings of NE dynamics revealed unique oscillations in NE release during non–rapid eye movement (NREM) sleep, which may play a critical role in shaping the microarchitecture of sleep (110). With respect to DA sensors, Hasegawa et al. (111) measured DA release in the basolateral amygdala during the sleep–wake cycle and found that a transient increase in dopaminergic activity during NREM sleep is essential for transitioning from NREM sleep to REM sleep. Finally, several groups have studied other extracellular neurochemicals, including ACh (112), serotonin (91), DA, ATP (113), and orexin (114).

Fluorescent sensors can also provide remarkably rich information regarding the spatial dynamics of neurochemicals. To study neuromodulation at cellular resolution, investigators have applied one-photon and multiphoton microscopy to neurochemical imaging. For example, the iGluSnFR series has successfully been used to image glutamate release in vivo. The recently developed iGluSnFR3, which has a larger dynamic range when excited using a two-photon laser, has been used to monitor glutamate release in individual synaptic boutons (84) (**Figure 3*e***). Using a highly sensitive ATP sensor, Wu et al. (95) found a localized increase in ATP release during lipopolysaccharide-induced systemic inflammation; a further analysis indicated that the early release of ATP in the cortex occurs near blood vessels. Patriarchi et al. (90, 115) used dLight sensors to measure cortical DA release during a reward-associated visuomotor task and found that DA release was linked to specific motor or reward behaviors, with a spatially heterogeneous distribution.

Interestingly, NM signals can even be measured in deep brain structures by implanting imaging cannulas. For example, Hamid et al. (116) combined Ca^{2+} imaging with DA imaging in the mouse dorsal striatum and observed wavelike DA signals during instrumental and Pavlovian tasks, with opposing wave directions. This observation suggests that the spatiotemporal propagation of DA signaling is critical for shaping learning behaviors. Using miniature two-photon microscopy, which capitalizes on the high spatial sensitivity of neurochemical sensors in freely moving mice while behaving naturally, Jing et al. (112) observed increased ACh release during locomotion, but not in response to visual or auditory stimuli.

At the other end of the scale, measuring changes in neurochemicals at the mesoscopic level has been instrumental in addressing questions regarding how various brain regions coordinate to support overall brain function. Although mesoscopic imaging techniques do not offer single-cell resolution, they facilitate the simultaneous monitoring of neurochemicals over relatively large areas (117). In early studies, voltage-sensitive dyes were widely used with wide-field imaging to monitor cortical function in vivo (118, 119), revealing patterns of spontaneous and sensory-evoked activity across large regions. The widespread use of GECIs now enables measurements of neuronal Ca^{2+} signals throughout the entire dorsal cortex. Neurochemical sensors for NTs and NMs were recently used to monitor changes in neurochemicals on a large scale.

For example, Lohani et al. (120) used dual-color wide-field imaging to study the relationship between ACh and Ca^{2+} signaling throughout the dorsal cortex and found spatially heterogeneous cholinergic activity that was differentially associated with distinct behavioral states. In addition, using wide-field imaging, we recently capitalized on the rapid kinetics of neurochemical sensors and found wavelike propagation of Ca^{2+}, serotonin, and endocannabinoids during seizures (121).

Several NM sensors have also been used to measure neurochemicals in *Drosophila* and zebrafish (89, 92, 95). For example, we recently imaged serotonin and ACh release in the *Drosophila* mushroom body (MB), which serves as the learning center, and found spatially heterogeneous serotonin signals that bidirectionally regulate the coincidence time window in a Pavlovian learning paradigm (122). In another study, Stahl et al. (123) examined olfactory learning in *Drosophila* and found bidirectional modulation of ACh signals in the MB that was specific to the valence of the learning event (i.e., aversive versus appetitive) and the MB compartment.

6. FUTURE PERSPECTIVES

The rapid development of genetically encoded sensors has in many ways revolutionized the field of neuroscience. However, single-FP-based sensors and their intensiometric imaging modalities have intrinsic limitations in terms of quantitative measurement and multiplexed imaging. In this section, we describe three novel imaging modalities and the corresponding sensor designs that aim to overcome these challenges.

6.1. Quantitative Imaging

Many of the currently popular neurochemical sensors used for in vivo imaging use a single fluorophore and rely heavily—if not entirely—on a change in fluorescence intensity to report ligand binding. Intensity-based measurements are affected by perturbations and extrinsic factors such as the local fluorophore concentration, wavelength-dependent light scattering, and fluctuations in excitation. Therefore, sensors based on intensity can report only qualitative, relative changes in the ligand of interest, irrespective of their basal concentration.

To overcome these limitations in the context of neurochemical sensors, the sensor's readout should be linked directly to ligand concentration. Although doing so remains a challenge, several strategies have been proposed. Each is discussed below.

6.1.1. Ratiometric sensors. Ratiometric sensors are characterized by a change in either their excitation or emission wavelength in response to a change in the sensor's state. Ideally, this change in excitation or emission wavelength should be determined solely by the number of ligand molecules bound to the sensors. Therefore, ratiometric sensors have an intrinsic reference system that can mitigate the unwanted effects of external factors and can effectively provide a sensitive, quantitative measurement of the corresponding ligand. Typically, intensities at two or more wavelengths of either the excitation or emission spectrum are measured. Ratiometric sensors are therefore categorized into excitation and emission ratiometric sensors.

With excitation ratiometric sensors, the sensor's excitation curve shifts when bound to the respective ligand. Thus, by exciting the sensor using two distinct wavelengths and recording a fixed emission wavelength, one can calculate the emission ratio between the two excitation wavelengths and determine the sensor's state, which—when calibrated properly—should correspond to the ligand concentration (**Figure 4*a***). The idea of excitation ratiometric sensors emerged from the Ca^{2+} dye fura-2, developed by Tsien and collaborators in 1985 (46). This dye's excitation peak undergoes a blue shift from ∼362 nm to ∼340 nm when saturated with Ca^{2+}, and it has been widely

used to image changes in Ca^{2+} concentration. Although fura-2 is not a genetically encoded sensor, the underlying principle has been used to develop a number of excitation ratiometric sensors (50, 124–127). In theory, this approach can be used to determine ligand concentration, with the calculated ratio corresponding to the percentage of chromophores residing in each of the neutral and

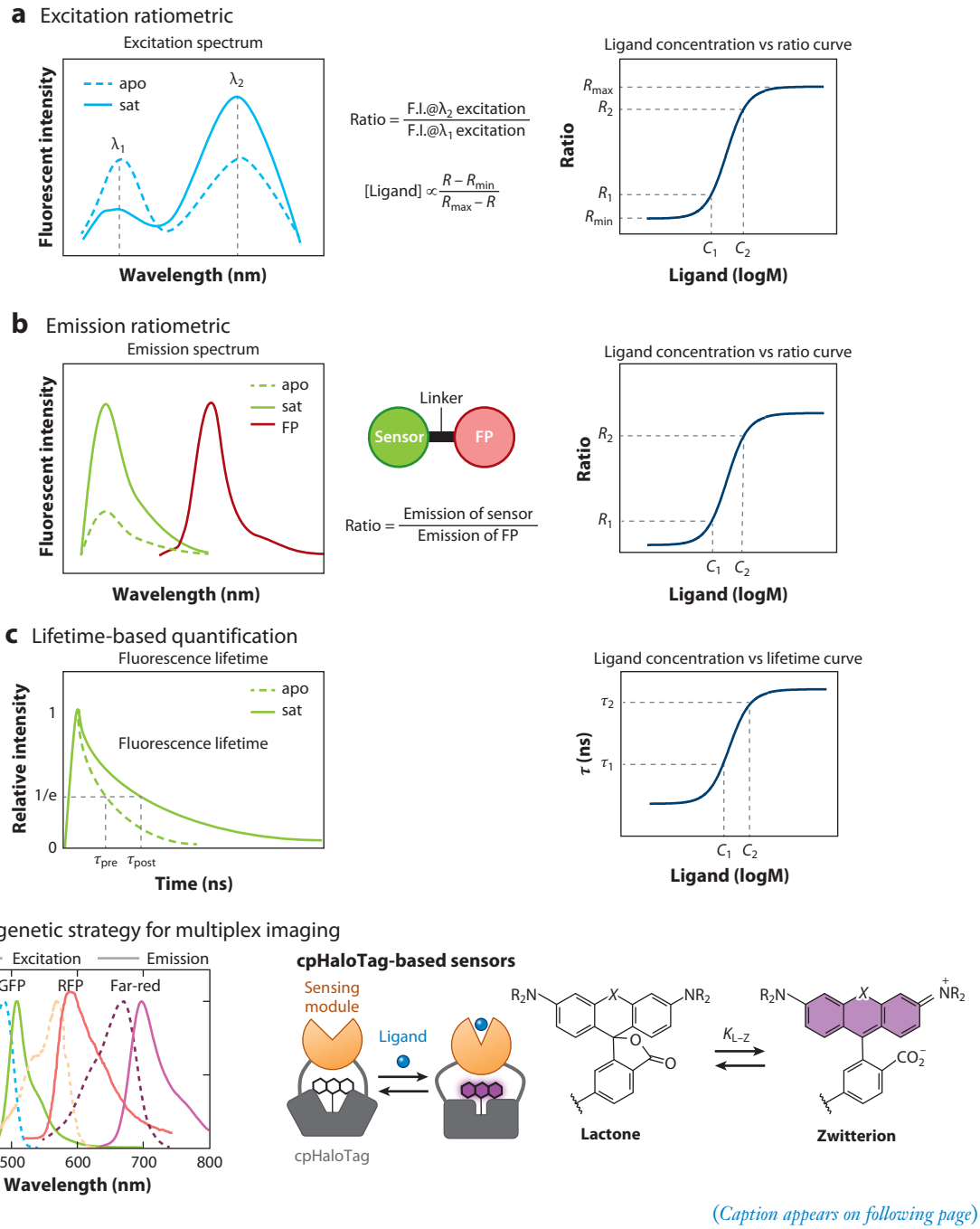

(Caption appears on following page)

Figure 4 (*Figure appears on preceding page*)

Developments in neurochemical sensors for use in quantitative measurements and multiplex imaging. (*a*) Schematic representation of excitation ratiometric sensors in ligand-free (apo) and ligand-saturated (sat) states. (*Left*) Representative excitation spectrum of an excitation ratiometric sensor. The sensor is excited using two wavelengths (λ_1 and λ_2) with different absorptions, and the emission light is collected from each excitation wavelength. (*Right*) The ratio between the emission intensity excited by wavelength λ_1 and the emission intensity excited by λ_2 can then be used to quantify ligand concentration. (*b*) Schematic representation of emission ratiometric sensors. By fusing a constitutively fluorescing FP to an intensiometric sensor serving as a reference, one can use the emission from two chromophores to calculate an emission ratio and quantify ligand concentration. (*c*) Principle of FLIM-based quantification, in which a difference in fluorescence lifetime directly corresponds to ligand concentration. (*d*) Schematic diagram of using a HaloTag-based strategy in multiplex imaging. Ligand binding to the sensing domain induces a conformation change in the sensor, causing the equilibrium of the chromophore (rhodamine dye) in the sensor to shift to the fluorogenic zwitterion state and thereby increasing F.I. Abbreviations: cp, circularly permuted; F.I., fluorescence intensity; FLIM, fluorescence lifetime imaging microscopy; FP, fluorescent protein; GFP, green fluorescent protein; RFP, red fluorescent protein. Figure adapted from Reference 61.

ionized states. This approach can also help reduce the effects of differences in sensor expression levels and movement-related artifacts.

Emission ratiometric sensors typically use two distinct emission wavelengths; one changes in response to ligand binding, and the other is used as a fixed reference to minimize nonspecific perturbations (**Figure 4*b***). An emission radiometric sensor can be constructed by, for example, fusing a chemically stable FP with a spectrally distinguishable emission wavelength to an intensity-based sensor (128, 129). Alternatively, some sensors undergo a shift in their emission peak in response to ligand binding, allowing for ratiometric imaging (56). Despite their advantages, excitation and emission ratiometric sensors are still subject to wavelength-dependent scattering, and differences in experiment parameters (e.g., the excitation and/or emission wavelength) can also affect the signal readout.

6.1.2. Fluorescence lifetime–based sensors. Fluorescence lifetime is defined as the average time in which an excited fluorophore remains in the excited state. Because the number of photons emitted by a group of excited fluorophores decays exponentially, fluorescence lifetime is defined as the time it takes for the number of emitted photons to decrease to $1/e$ (or approximately 36.8%) of the original fluorescence. Unlike intensity-based measurements, fluorescence lifetime is independent of factors such as fluorophore concentration and excitation intensity and can be measured quantitatively using FLIM. Therefore, fluorescence lifetime measurements have intrinsic advantages over intensity measurements, as they can provide a robust signal readout that is relatively unaffected by external factors that would normally affect intensity. As a result, fluorescence lifetime may be suitable for quantitative measurements (**Figure 4*c***).

The idea of using fluorescence lifetime for quantitative imaging has a fairly long history; indeed, researchers first used this approach in the 1990s with pH-sensitive chemical dyes to quantitively measure intracellular pH in living cells (130). Much more recently, Zheng et al. (29) used the chemical dye Oregon green BAPTA-1 to map $[Ca^{2+}]_i$ in cultured neurons, acute brain slices, and living mice. Although genetically encoded fluorescence lifetime sensors have not yet been used for quantitative imaging, recent progress has brought this goal one step closer. For example, as noted above, the FRET-FLIM-based sensor cAMPFIRE developed by Massengill et al. (71) has a relatively robust lifetime readout lasting more than 1 month, an essential feature for future applications using quantitative imaging. In addition, van der Linden et al. (31) used a single-FP-based genetically encoded Ca^{2+} sensor as a lifetime-based biosensor to quantitatively image intracellular Ca^{2+}.

The commercial availability of specialized FLIM instruments is increasing, and studies are attempting to optimize these tools to increase the temporal resolution of FLIM microscopes. With these and other advances in both sensor development and imaging instruments, the use of

FLIM-based sensors and imaging techniques will likely lead to major advances in our ability to visualize and quantify neurochemicals.

6.2. Expanding the Spectra of Sensors for Use in Multiplex Imaging

The ability to use multiplex imaging to measure multiple neurochemicals simultaneously will represent a major step toward obtaining a comprehensive understanding of signaling in neural networks. To reach this goal, sensors must be developed with spectrally distinct spectra. Currently, most intensity-based sensors use cpGFP as the fluorophore, with an excitation peak at 488 nm and an emission peak at 507 nm (37), and some Ca^{2+}, cAMP, and DA sensors use red-shifted fluorophores, as discussed above. Developing sensors with unique spectra will allow researchers to perform multiplex imaging of neurochemicals, providing important new insights into complex neural processes. For example, red-shifted sensors in the far-red or near-infrared (NIR) region of the spectrum are needed to expand multiplex imaging. These sensors will also have practical advantages over existing sensors, including reduced light scattering and deeper tissue penetration, thereby facilitating their use in in vivo imaging.

One approach to developing genetically encoded far-red and NIR sensors involves the use of cpFPs with these spectral properties. Over the past two decades, several far-red and NIR FPs have been developed (131–136), and some of them have been used to generate genetically encoded sensors. Although these far-red and NIR sensors have been used for in vivo imaging in various organisms (137), they have a relatively low SNR. This is not unexpected, given that most far-red and NIR FPs have relatively low molecular brightness, which hinders their use in vivo. Therefore, steps to further optimize current far-red and NIR FPs should focus on increasing their brightness, and thereby increasing their functionality, particularly in vivo.

Another viable strategy is based on the combination of chemical dyes and chemically selective genetically encoded self-labeling proteins, which provides cellular specificity. Chemical dyes generally have higher molecular brightness and photostability compared with FPs; moreover, researchers have made strides toward increasing their solubility and their ability to cross cell membranes, as well as their ability to cross the blood–brain barrier, making them suitable for in vivo applications in the brain (138). For example, the Janelia fluor (JF) series of fluorescent dyes, developed by the Lavis group (139, 140) at Janelia Research Campus (Ashburn, Virginia), meets many of these requirements.

An array of genetically encoded self-labeling proteins has been developed to overcome the lack of cell specificity with chemical dyes (141–144). For example, HaloTag, which is derived from a bacterial haloalkane dehalogenase enzyme, binds specifically to synthetic HaloTag ligands that contain chloroalkane groups (141). Originally designed to label proteins, this strategy has been adapted to develop chemigenetic hybrid sensors, which combine cellular specificity with a high SNR (**Figure 4*d***). The genetically encoded voltage indicator Voltron, developed by the Schreiter group (145), uses the voltage-sensitive microbial rhodopsin Ace2N domain and the HaloTag protein. Upon the binding of HaloTag to a JF dye, a change in the cell's membrane potential induces a conformational change in the Ace2N domain, thereby altering FRET efficiency between the HaloTag–JF dye complex and Ace2N. Importantly, Voltron has been successfully used in several in vivo models, including mice, zebrafish larvae, and *Drosophila*. Furthermore, protein tags can be circularly permuted in a fashion similar to cpFPs to expose the chemical dyes and modulate their intensity, as demonstrated by the development of rHCaMP (146) and HaloCaMP (61).

These advances in chemigenetic hybrid sensors are paving the way toward the development of next-generation sensors designed to visualize neurochemicals. Choosing the ideal combination

of excitation and emission wavelengths will enable the addition of multiplex imaging to future studies.

7. CLOSING REMARKS

7.1. Limitations of Genetically Encoded Sensors

In this section, we discuss the limitations of current genetically encoded sensors. First, ethical concerns prohibit their use in humans, and such use is unlikely to be allowed in the foreseeable future. Second, existing intensiometric sensors provide information only about relative changes in chemical dynamics, without offering absolute concentration measurements. Third, the capability for multichannel imaging is hindered by the lack of spectrally orthogonal sensors, as most sensors are based on GFP. Fourth, deep brain imaging remains a challenge because of the complex procedures involved in gradient index lens implantation and the potential tissue damage that accompanies it. Although three-photon imaging allows for deeper tissue penetration (up to 1.6 mm), it also presents a new challenge in the development of customized sensors for multiphoton imaging (147–149).

7.2. Future Directions for Developing and Using Genetically Encoded Sensors

Thanks to numerous advances in the development of genetically encoded sensors, researchers can now observe dynamic changes in numerous neurochemicals at an unprecedented level of spatial and temporal resolution. Furthermore, GPCR-based sensors hold significant promise for use in drug screening studies, particularly because they are widely targeted by many therapeutic compounds.

Although the development of neurochemical sensors has made significant progress, several key challenges remain, including expanding the repertoire of sensors, achieving extensive multiplex imaging, and translating sensor readouts into quantitative measurements (e.g., ligand concentration, pH); reaching these important goals will likely require innovation and collaboration. Fortunately, the fields of biology and physiology are witnessing a surge in technologies and tools that can facilitate sensor development and help unravel the mysteries surrounding the role of neurochemicals in the central nervous system. With respect to developing new sensors, structure–function predictions based on computational algorithms (86) and insights provided by structural biologists can be used as a frame of reference for the rational design, evolution, and optimization of these sensors. For end users, genetically encoded sensors can be exploited using a wide range of tools, including—but not limited to—optogenetic and chemigenetic manipulation, pharmacology, and CRISPR/Cas9-mediated gene editing. By integrating these tools and engaging in multidisciplinary collaborations, we can push past the boundaries around our knowledge of neurochemicals and their role in both health and disease.

DISCLOSURE STATEMENT

Y.L. is listed as an inventor on a pending patent application filed by Peking University (international patent number PCT/CN2018/107533), the value of which might be affected by this publication. The other authors are not aware of any affiliations, memberships, funding, or financial holdings that might be perceived as affecting the objectivity of this review.

ACKNOWLEDGMENTS

The authors thank Dr. Kaspar Podgorski for providing **Figure 3*e*** and the members of the Li lab for helpful discussions. This research was supported by the Beijing Municipal Science &

Technology Commission (Z181100001318002 and Z181100001518004), the National Natural Science Foundation of China (81821092), the National Key Research and Development Program of China (2020YFE0204000), the Feng Foundation of Biomedical Research, the Peking–Tsinghua Center for Life Sciences and the State Key Laboratory of Membrane Biology at Peking University School of Life Sciences, and the US National Institutes of Health Brain Research Through Advancing Innovative Neurotechnologies (BRAIN) Initiative (NS103558 to Y.L.).

LITERATURE CITED

1. Clapham DE. 2007. Calcium signaling. *Cell* 131:1047–58
2. Sudhof TC. 2004. The synaptic vesicle cycle. *Annu. Rev. Neurosci.* 27:509–47
3. Grienberger C, Konnerth A. 2012. Imaging calcium in neurons. *Neuron* 73:862–85
4. Smith SJ, Sümbül U, Graybuck LT, Collman F, Seshamani S, et al. 2019. Single-cell transcriptomic evidence for dense intracortical neuropeptide networks. *eLife* 8:e47889
5. Burnstock G. 2014. Purinergic signalling: from discovery to current developments. *Exp. Physiol.* 99:16–34
6. Castillo PE, Younts TJ, Chávez AE, Hashimotodani Y. 2012. Endocannabinoid signaling and synaptic function. *Neuron* 76:70–81
7. Sassone-Corsi P. 2012. The cyclic AMP pathway. *Cold Spring Harb. Perspect. Biol.* 4:a011148
8. Calebiro D, Maiellaro I. 2014. cAMP signaling microdomains and their observation by optical methods. *Front. Cell Neurosci.* 8:350
9. Bowery NG, Smart TG. 2006. GABA and glycine as neurotransmitters: a brief history. *Br. J. Pharmacol.* 147(Suppl. 1):S109–19
10. Reiner A, Levitz J. 2018. Glutamatergic signaling in the central nervous system: ionotropic and metabotropic receptors in concert. *Neuron* 98:1080–98
11. Fejtl M, Carpenter DO. 1996. Single-channel studies in molluscan neurons. In *Ion Channels*, ed. T Narahashi, pp. 333–76. Boston: Springer
12. Greengard P. 2001. The neurobiology of slow synaptic transmission. *Science* 294:1024–30
13. Nadim F, Bucher D. 2014. Neuromodulation of neurons and synapses. *Curr. Opin. Neurobiol.* 29:48–56
14. Marder E. 2012. Neuromodulation of neuronal circuits: back to the future. *Neuron* 76:1–11
15. Wu Z, Lin D, Li Y. 2022. Pushing the frontiers: tools for monitoring neurotransmitters and neuromodulators. *Nat. Rev. Neurosci.* 23:257–74
16. Wang H, Jing M, Li Y. 2018. Lighting up the brain: genetically encoded fluorescent sensors for imaging neurotransmitters and neuromodulators. *Curr. Opin. Neurobiol.* 50:171–78
17. Sabatini BL, Tian L. 2020. Imaging neurotransmitter and neuromodulator dynamics in vivo with genetically encoded indicators. *Neuron* 108:17–32
18. Dong C, Zheng Y, Long-Iyer K, Wright EC, Li Y, Tian L. 2022. Fluorescence imaging of neural activity, neurochemical dynamics, and drug-specific receptor conformation with genetically encoded sensors. *Annu. Rev. Neurosci.* 45:273–94
19. Jean-Martin B, Raul RG. 2011. The physiology, signaling, and pharmacology of dopamine receptors. *Pharmacol. Rev.* 63:182–217
20. Surmeier DJ, Ding J, Day M, Wang Z, Shen W. 2007. D1 and D2 dopamine-receptor modulation of striatal glutamatergic signaling in striatal medium spiny neurons. *Trends Neurosci.* 30:228–35
21. Jakob KD, Kjartan FH, Rune WB, Jørn DH. 2010. Influence of phasic and tonic dopamine release on receptor activation. *J. Neurosci.* 30:14273–83
22. Keeler JF, Pretsell DO, Robbins TW. 2014. Functional implications of dopamine D1 versus D2 receptors: a 'prepare and select' model of the striatal direct versus indirect pathways. *Neuroscience* 282:156–75
23. Carhart-Harris RL, Nutt DJ. 2017. Serotonin and brain function: a tale of two receptors. *J. Psychopharmacol.* 31:1091–120
24. Shimomura O, Johnson FH, Saiga Y. 1962. Extraction, purification and properties of aequorin, a bioluminescent protein from the luminous hydromedusan, *Aequorea*. *J. Cell Comp. Physiol.* 59:223–39
25. Chalfie M, Tu Y, Euskirchen G, Ward WW, Prasher DC. 1994. Green fluorescent protein as a marker for gene expression. *Science* 263:802–5

26. Chudakov DM, Lukyanov S, Lukyanov KA. 2005. Fluorescent proteins as a toolkit for in vivo imaging. *Trends Biotechnol.* 23:605–13
27. Datta R, Heaster TM, Sharick JT, Gillette AA, Skala MC. 2020. Fluorescence lifetime imaging microscopy: fundamentals and advances in instrumentation, analysis, and applications. *J. Biomed. Opt.* 25:071203
28. Becker W. 2012. Fluorescence lifetime imaging—techniques and applications. *J. Microsc.* 247:119–36
29. Zheng K, Bard L, Reynolds JP, King C, Jensen TP, et al. 2015. Time-resolved imaging reveals heterogeneous landscapes of nanomolar Ca^{2+} in neurons and astroglia. *Neuron* 88:277–88
30. Linders PTA, Ioannidis M, ter Beest M, van den Bogaart G. 2022. Fluorescence lifetime imaging of pH along the secretory pathway. *ACS Chem. Biol.* 17:240–51
31. van der Linden FH, Mahlandt EK, Arts JJG, Beumer J, Puschhof J, et al. 2021. A turquoise fluorescence lifetime–based biosensor for quantitative imaging of intracellular calcium. *Nat. Commun.* 12:7159
32. Massengill CI, Day-Cooney J, Mao T, Zhong H. 2021. Genetically encoded sensors towards imaging cAMP and PKA activity in vivo. *J. Neurosci. Methods* 362:109298
33. Rennick JJ, Nowell CJ, Pouton CW, Johnston APR. 2022. Resolving subcellular pH with a quantitative fluorescent lifetime biosensor. *Nat. Commun.* 13:6023
34. Carlson HJ, Campbell RE. 2009. Genetically encoded FRET-based biosensors for multiparameter fluorescence imaging. *Curr. Opin. Biotechnol.* 20:19–27
35. Wang Q, Shui B, Kotlikoff MI, Sondermann H. 2008. Structural basis for calcium sensing by GCaMP2. *Structure* 16:1817–27
36. Akerboom J, Rivera JDV, Guilbe MMR, Malavé ECA, Hernandez HH, et al. 2009. Crystal structures of the GCaMP calcium sensor reveal the mechanism of fluorescence signal change and aid rational design. *J. Biol. Chem.* 284:6455–64
37. Tsien RY. 1998. The green fluorescent protein. *Annu. Rev. Biochem.* 67:509–44
38. Akerboom J, Carreras Calderon N, Tian L, Wabnig S, Prigge M, et al. 2013. Genetically encoded calcium indicators for multi-color neural activity imaging and combination with optogenetics. *Front. Mol. Neurosci.* 6:2
39. Ding J, Luo AF, Hu L, Wang D, Shao F. 2014. Structural basis of the ultrasensitive calcium indicator GCaMP6. *Sci. China Life Sci.* 57:269–74
40. Shivange AV, Borden PM, Muthusamy AK, Nichols AL, Bera K, et al. 2019. Determining the pharmacokinetics of nicotinic drugs in the endoplasmic reticulum using biosensors. *J. Gen. Physiol.* 151:738–57
41. Subach OM, Sotskov VP, Plusnin VV, Gruzdeva AM, Barykina NV, et al. 2020. Novel genetically encoded bright positive calcium indicator NCaMP7 based on the mNeonGreen fluorescent protein. *Int. J. Mol. Sci.* 21:1644
42. Wang L, Wu C, Peng W, Zhou Z, Zeng J, et al. 2022. A high-performance genetically encoded fluorescent indicator for in vivo cAMP imaging. *Nat. Commun.* 13:5363
43. Ashley CC, Ridgway EB. 1968. Simultaneous recording of membrane potential, calcium transient and tension in single muscle fibres. *Nature* 219:1168–69
44. Hallett M, Carbone E. 1972. Studies of calcium influx into squid giant axons with aequorin. *J. Cell. Physiol.* 80:219–26
45. Zhou X, Belavek KJ, Miller EW. 2021. Origins of Ca^{2+} imaging with fluorescent indicators. *Biochemistry* 60:3547–54
46. Grynkiewicz G, Poenie M, Tsien RY. 1985. A new generation of Ca^{2+} indicators with greatly improved fluorescence properties. *J. Biol. Chem.* 260:3440–50
47. Miyawaki A, Llopis J, Heim R, McCaffery JM, Adams JA, et al. 1997. Fluorescent indicators for Ca^{2+} based on green fluorescent proteins and calmodulin. *Nature* 388:882–87
48. Thestrup T, Litzlbauer J, Bartholomäus I, Mues M, Russo L, et al. 2014. Optimized ratiometric calcium sensors for functional in vivo imaging of neurons and T lymphocytes. *Nat. Methods* 11:175–82
49. Mank M, Reiff DF, Heim N, Friedrich MW, Borst A, Griesbeck O. 2006. A FRET-based calcium biosensor with fast signal kinetics and high fluorescence change. *Biophys. J.* 90:1790–96
50. Nagai T, Sawano A, Park ES, Miyawaki A. 2001. Circularly permuted green fluorescent proteins engineered to sense Ca^{2+}. *PNAS* 98:3197–202

51. Nakai J, Ohkura M, Imoto K. 2001. A high signal-to-noise Ca^{2+} probe composed of a single green fluorescent protein. *Nat. Biotechnol.* 19:137–41
52. Baird GS, Zacharias DA, Tsien RY. 1999. Circular permutation and receptor insertion within green fluorescent proteins. *PNAS* 96:11241–46
53. Chen T-W, Wardill TJ, Sun Y, Pulver SR, Renninger SL, et al. 2013. Ultrasensitive fluorescent proteins for imaging neuronal activity. *Nature* 499:295–300
54. Li J, Shang Z, Chen J-H, Gu W, Yao L, et al. 2023. Engineering of NEMO as calcium indicators with large dynamics and high sensitivity. *Nat. Methods* 20:918–24
55. Zhang Y, Rózsa M, Liang Y, Bushey D, Wei Z, et al. 2023. Fast and sensitive GCaMP calcium indicators for imaging neural populations. *Nature* 615:884–91
56. Zhao Y, Araki S, Wu J, Teramoto T, Chang YF, et al. 2011. An expanded palette of genetically encoded Ca^{2+} indicators. *Science* 333:1888–91
57. Inoue M, Takeuchi A, Manita S, Horigane SI, Sakamoto M, et al. 2019. Rational engineering of XCaMPs, a multicolor GECI suite for in vivo imaging of complex brain circuit dynamics. *Cell* 177:1346–60.e24
58. Dana H, Mohar B, Sun Y, Narayan S, Gordus A, et al. 2016. Sensitive red protein calcium indicators for imaging neural activity. *eLife* 5:e12727
59. Qian Y, Piatkevich KD, Mc Larney B, Abdelfattah AS, Mehta S, et al. 2019. A genetically encoded near-infrared fluorescent calcium ion indicator. *Nat. Methods* 16:171–74
60. Shemetov AA, Monakhov MV, Zhang Q, Canton-Josh JE, Kumar M, et al. 2021. A near-infrared genetically encoded calcium indicator for in vivo imaging. *Nat. Biotechnol.* 39:368–77
61. Deo C, Abdelfattah AS, Bhargava HK, Berro AJ, Falco N, et al. 2021. The HaloTag as a general scaffold for far-red tunable chemigenetic indicators. *Nat. Chem. Biol.* 17:718–23
62. Adams SR, Harootunian AT, Buechler YJ, Taylor SS, Tsien RY. 1991. Fluorescence ratio imaging of cyclic AMP in single cells. *Nature* 349:694–97
63. Zaccolo M, De Giorgi F, Cho CY, Feng L, Knapp T, et al. 2000. A genetically encoded, fluorescent indicator for cyclic AMP in living cells. *Nat. Cell Biol.* 2:25–29
64. Zaccolo M, Pozzan T. 2002. Discrete microdomains with high concentration of cAMP in stimulated rat neonatal cardiac myocytes. *Science* 295:1711–15
65. Mongillo M, McSorley T, Evellin S, Sood A, Lissandron V, et al. 2004. Fluorescence resonance energy transfer–based analysis of cAMP dynamics in live neonatal rat cardiac myocytes reveals distinct functions of compartmentalized phosphodiesterases. *Circ. Res.* 95:67–75
66. Lissandron V, Terrin A, Collini M, D'Alfonso L, Chirico G, et al. 2005. Improvement of a FRET-based indicator for cAMP by linker design and stabilization of donor–acceptor interaction. *J. Mol. Biol.* 354:546–55
67. Ponsioen B, Zhao J, Riedl J, Zwartkruis F, van der Krogt G, et al. 2004. Detecting cAMP-induced Epac activation by fluorescence resonance energy transfer: Epac as a novel cAMP indicator. *EMBO Rep.* 5:1176–80
68. Nikolaev VO, Bünemann M, Hein L, Hannawacker A, Lohse MJ. 2004. Novel single chain cAMP sensors for receptor-induced signal propagation. *J. Biol. Chem.* 279:37215–18
69. DiPilato LM, Cheng X, Zhang J. 2004. Fluorescent indicators of cAMP and Epac activation reveal differential dynamics of cAMP signaling within discrete subcellular compartments. *PNAS* 101:16513–18
70. Mukherjee S, Jansen V, Jikeli JF, Hamzeh H, Alvarez L, et al. 2016. A novel biosensor to study cAMP dynamics in cilia and flagella. *eLife* 5:e14052
71. Massengill CI, Bayless-Edwards L, Ceballos CC, Cebul ER, Cahill J, et al. 2022. Sensitive genetically encoded sensors for population and subcellular imaging of cAMP in vivo. *Nat. Methods* 19:1461–71
72. Liu W, Liu C, Ren PG, Chu J, Wang L. 2022. An improved genetically encoded fluorescent cAMP indicator for sensitive cAMP imaging and fast drug screening. *Front. Pharmacol.* 13:902290
73. Kitaguchi T, Oya M, Wada Y, Tsuboi T, Miyawaki A. 2013. Extracellular calcium influx activates adenylate cyclase 1 and potentiates insulin secretion in MIN6 cells. *Biochem. J.* 450:365–73
74. Ohta Y, Furuta T, Nagai T, Horikawa K. 2018. Red fluorescent cAMP indicator with increased affinity and expanded dynamic range. *Sci. Rep.* 8:1866
75. Castro LRV, Guiot E, Polito M, Paupardin-Tritsch D, Vincent P. 2014. Decoding spatial and temporal features of neuronal cAMP/PKA signaling with FRET biosensors. *Biotechnol. J.* 9:192–202

76. Gorshkov K, Zhang J. 2014. Visualization of cyclic nucleotide dynamics in neurons. *Front. Cell Neurosci.* 8:395
77. Wong DT, Perry KW, Bymaster FP. 2005. The discovery of fluoxetine hydrochloride (Prozac). *Nat. Rev. Drug Discov.* 4:764–74
78. Dwyer MA, Hellinga HW. 2004. Periplasmic binding proteins: a versatile superfamily for protein engineering. *Curr. Opin. Struct. Biol.* 14:495–504
79. Okumoto S, Looger LL, Micheva KD, Reimer RJ, Smith SJ, Frommer WB. 2005. Detection of glutamate release from neurons by genetically encoded surface-displayed FRET nanosensors. *PNAS* 102:8740–45
80. Tsien RY. 2005. Building and breeding molecules to spy on cells and tumors. *FEBS Lett.* 579:927–32
81. Hires SA, Zhu Y, Tsien RY. 2008. Optical measurement of synaptic glutamate spillover and reuptake by linker optimized glutamate-sensitive fluorescent reporters. *PNAS* 105:4411–16
82. Marvin JS, Borghuis BG, Tian L, Cichon J, Harnett MT, et al. 2013. An optimized fluorescent probe for visualizing glutamate neurotransmission. *Nat. Methods* 10:162–70
83. Marvin JS, Scholl B, Wilson DE, Podgorski K, Kazemipour A, et al. 2018. Stability, affinity, and chromatic variants of the glutamate sensor iGluSnFR. *Nat. Methods* 15:936–39
84. Aggarwal A, Liu R, Chen Y, Ralowicz AJ, Bergerson SJ, et al. 2023. Glutamate indicators with improved activation kinetics and localization for imaging synaptic transmission. *Nat. Methods* 20:925–34
85. Philip MB, Peng Z, Amol VS, Jonathan SM, Joseph C, et al. 2020. A fast genetically encoded fluorescent sensor for faithful in vivo acetylcholine detection in mice, fish, worms and flies. bioRxiv 2020.02.07.939504. **https://doi.org/10.1101/2020.02.07.93950**
86. Unger EK, Keller JP, Altermatt M, Liang R, Matsui A, et al. 2020. Directed evolution of a selective and sensitive serotonin sensor via machine learning. *Cell* 183:1986–2002.e26
87. Marvin JS, Shimoda Y, Magloire V, Leite M, Kawashima T, et al. 2019. A genetically encoded fluorescent sensor for in vivo imaging of GABA. *Nat. Methods* 16:763–70
88. Weis WI, Kobilka BK. 2018. The molecular basis of G protein–coupled receptor activation. *Annu. Rev. Biochem.* 87:897–919
89. Sun F, Zeng J, Jing M, Zhou J, Feng J, et al. 2018. A genetically encoded fluorescent sensor enables rapid and specific detection of dopamine in flies, fish, and mice. *Cell* 174:481–96.e19
90. Patriarchi T, Cho JR, Merten K, Howe MW, Marley A, et al. 2018. Ultrafast neuronal imaging of dopamine dynamics with designed genetically encoded sensors. *Science* 360:eaat4422
91. Wan J, Peng W, Li X, Qian T, Song K, et al. 2021. A genetically encoded sensor for measuring serotonin dynamics. *Nat. Neurosci.* 24:746–52
92. Feng J, Zhang C, Lischinsky JE, Jing M, Zhou J, et al. 2019. A genetically encoded fluorescent sensor for rapid and specific in vivo detection of norepinephrine. *Neuron* 102:745–61.e8
93. Dong H, Li M, Yan Y, Qian T, Lin Y, et al. 2023. Genetically encoded sensors for measuring histamine release both in vitro and in vivo. *Neuron* 111:1564–76.e6
94. Dong C, Ly C, Dunlap LE, Vargas MV, Sun J, et al. 2021. Psychedelic-inspired drug discovery using an engineered biosensor. *Cell* 184:2779–92.e18
95. Wu Z, He K, Chen Y, Li H, Pan S, et al. 2022. A sensitive GRAB sensor for detecting extracellular ATP in vitro and in vivo. *Neuron* 110:770–82.e5
96. Peng W, Wu Z, Song K, Zhang S, Li Y, Xu M. 2020. Regulation of sleep homeostasis mediator adenosine by basal forebrain glutamatergic neurons. *Science* 369:eabb0556
97. Dong A, He K, Dudok B, Farrell JS, Guan W, et al. 2022. A fluorescent sensor for spatiotemporally resolved imaging of endocannabinoid dynamics in vivo. *Nat. Biotechnol.* 40:787–98
98. Ino D, Tanaka Y, Hibino H, Nishiyama M. 2022. A fluorescent sensor for real-time measurement of extracellular oxytocin dynamics in the brain. *Nat. Methods* 19:1286–94
99. Qian T, Wang H, Wang P, Geng L, Mei L, et al. 2023. A genetically encoded sensor measures temporal oxytocin release from different neuronal compartments. *Nat. Biotechnol.* 41:944–57
100. Cui G, Jun SB, Jin X, Pham MD, Vogel SS, et al. 2013. Concurrent activation of striatal direct and indirect pathways during action initiation. *Nature* 494:238–42
101. Yang G, Pan F, Parkhurst CN, Grutzendler J, Gan W-B. 2010. Thinned-skull cranial window technique for long-term imaging of the cortex in live mice. *Nat. Protoc.* 5:201–8

102. Zhao Y-J, Yu T-T, Zhang C, Li Z, Luo Q-M, et al. 2018. Skull optical clearing window for in vivo imaging of the mouse cortex at synaptic resolution. *Light Sci. Appl.* 7:17153
103. Murray TA, Levene MJ. 2012. Singlet gradient index lens for deep in vivo multiphoton microscopy. *J. Biomed. Opt.* 17:021106
104. Zong W, Wu R, Li M, Hu Y, Li Y, et al. 2017. Fast high-resolution miniature two-photon microscopy for brain imaging in freely behaving mice. *Nat. Methods* 14:713–19
105. Zong W, Wu R, Chen S, Wu J, Wang H, et al. 2021. Miniature two-photon microscopy for enlarged field-of-view, multi-plane and long-term brain imaging. *Nat. Methods* 18:46–49
106. Dai B, Sun F, Tong X, Ding Y, Kuang A, et al. 2022. Responses and functions of dopamine in nucleus accumbens core during social behaviors. *Cell Rep.* 40:111246
107. Zhang SX, Lutas A, Yang S, Diaz A, Fluhr H, et al. 2021. Hypothalamic dopamine neurons motivate mating through persistent cAMP signalling. *Nature* 597:245–49
108. Scammell TE, Arrigoni E, Lipton JO. 2017. Neural circuitry of wakefulness and sleep. *Neuron* 93:747–65
109. Brown RE, Basheer R, McKenna JT, Strecker RE, McCarley RW. 2012. Control of sleep and wakefulness. *Physiol. Rev.* 92:1087–187
110. Kjaerby C, Andersen M, Hauglund N, Untiet V, Dall C, et al. 2022. Memory-enhancing properties of sleep depend on the oscillatory amplitude of norepinephrine. *Nat. Neurosci.* 25:1059–70
111. Hasegawa E, Miyasaka A, Sakurai K, Cherasse Y, Li Y, Sakurai T. 2022. Rapid eye movement sleep is initiated by basolateral amygdala dopamine signaling in mice. *Science* 375:994–1000
112. Jing M, Li Y, Zeng J, Huang P, Skirzewski M, et al. 2020. An optimized acetylcholine sensor for monitoring in vivo cholinergic activity. *Nat. Methods* 17:1139–46
113. Peng W, Liu X, Ma G, Wu Z, Wang Z, et al. 2023. Adenosine-independent regulation of the sleep–wake cycle by astrocyte activity. *Cell Discov.* 9:16
114. Duffet L, Kosar S, Panniello M, Viberti B, Bracey E, et al. 2022. A genetically encoded sensor for in vivo imaging of orexin neuropeptides. *Nat. Methods* 19:231–41
115. Patriarchi T, Cho JR, Merten K, Howe MW, Marley A, et al. 2018. Ultrafast neuronal imaging of dopamine dynamics with designed genetically encoded sensors. *Science* 360:aat4422
116. Hamid AA, Frank MJ, Moore CI. 2021. Wave-like dopamine dynamics as a mechanism for spatiotemporal credit assignment. *Cell* 184:2733–49.e16
117. Nietz AK, Popa LS, Streng ML, Carter RE, Kodandaramaiah SB, Ebner TJ. 2022. Wide-field calcium imaging of neuronal network dynamics in vivo. *Biology* 11:1601
118. Ferezou I, Haiss F, Gentet LJ, Aronoff R, Weber B, Petersen CCH. 2007. Spatiotemporal dynamics of cortical sensorimotor integration in behaving mice. *Neuron* 56:907–23
119. Petersen CCH. 2007. The functional organization of the barrel cortex. *Neuron* 56:339–55
120. Lohani S, Moberly AH, Benisty H, Landa B, Jing M, et al. 2022. Spatiotemporally heterogeneous coordination of cholinergic and neocortical activity. *Nat. Neurosci.* 25:1706–13
121. Fei D, Jinxia W, Guochuan L, Hui D, Xiju X, et al. 2023. Dual-color GRAB sensors for monitoring spatiotemporal serotonin release in vivo. bioRxiv 2023.05.27.542566. **https://doi.org/10.1101/2023.05.27.542566**
122. Zeng J, Li X, Zhang R, Lv M, Wang Y, et al. 2023. Local 5-HT signaling bi-directionally regulates the coincidence time window for associative learning. *Neuron* 111:1118–35.e5
123. Stahl A, Noyes NC, Boto T, Botero V, Broyles CN, et al. 2022. Associative learning drives longitudinally graded presynaptic plasticity of neurotransmitter release along axonal compartments. *eLife* 11:e76712
124. Wu J, Abdelfattah AS, Miraucourt LS, Kutsarova E, Ruangkittisakul A, et al. 2014. A long Stokes shift red fluorescent Ca^{2+} indicator protein for two-photon and ratiometric imaging. *Nat. Commun.* 5:5262
125. Mehta S, Zhang Y, Roth RH, Zhang J-F, Mo A, et al. 2018. Single-fluorophore biosensors for sensitive and multiplexed detection of signalling activities. *Nat. Cell Biol.* 20:1215–25
126. Zhao Y, Bushey D, Zhao Y, Schreiter ER, Harrison DJ, et al. 2018. Inverse-response Ca^{2+} indicators for optogenetic visualization of neuronal inhibition. *Sci. Rep.* 8:11758
127. Barykina NV, Sotskov VP, Gruzdeva AM, Wu YK, Portugues R, et al. 2020. FGCaMP7, an improved version of fungi-based ratiometric calcium indicator for in vivo visualization of neuronal activity. *Int. J. Mol. Sci.* 21:3012

128. Cho J-H, Swanson CJ, Chen J, Li A, Lippert LG, et al. 2017. The GCaMP-R family of genetically encoded ratiometric calcium indicators. *ACS Chem. Biol.* 12:1066–74
129. Ast C, Foret J, Oltrogge LM, De Michele R, Kleist TJ, et al. 2017. Ratiometric Matryoshka biosensors from a nested cassette of green- and orange-emitting fluorescent proteins. *Nat. Commun.* 8:431
130. Sandrers R, Draaijer A, Gerritsen HC, Houpt PM, Levine YK. 1995. Quantitative pH imaging in cells using confocal fluorescence lifetime imaging microscopy. *Anal. Biochem.* 227:302–8
131. Lin MZ, McKeown MR, Ng H-L, Aguilera TA, Shaner NC, et al. 2009. Autofluorescent proteins with excitation in the optical window for intravital imaging in mammals. *Chem. Biol.* 16:1169–79
132. Morozova KS, Piatkevich KD, Gould TJ, Zhang J, Bewersdorf J, Verkhusha VV. 2010. Far-red fluorescent protein excitable with red lasers for flow cytometry and superresolution STED nanoscopy. *Biophys. J.* 99:L13–15
133. Shcherbakova DM, Verkhusha VV. 2013. Near-infrared fluorescent proteins for multicolor in vivo imaging. *Nat. Methods* 10:751–54
134. Chu J, Haynes RD, Corbel SY, Li P, González-González E, et al. 2014. Non-invasive intravital imaging of cellular differentiation with a bright red–excitable fluorescent protein. *Nat. Methods* 11:572–78
135. Shcherbakova DM, Cox Cammer N, Huisman TM, Verkhusha VV, Hodgson L. 2018. Direct multiplex imaging and optogenetics of Rho GTPases enabled by near-infrared FRET. *Nat. Chem. Biol.* 14:591–600
136. Wannier TM, Gillespie SK, Hutchins N, McIsaac RS, Wu S-Y, et al. 2018. Monomerization of far-red fluorescent proteins. *PNAS* 115:E11294–301
137. Qian Y, Cosio DMO, Piatkevich KD, Aufmkolk S, Su W-C, et al. 2020. Improved genetically encoded near-infrared fluorescent calcium ion indicators for in vivo imaging. *PLOS Biol.* 18:e3000965
138. Keller SG, Kamiya M, Urano Y. 2020. Recent progress in small spirocyclic, xanthene-based fluorescent probes. *Molecules* 25:5964
139. Grimm JB, English BP, Chen J, Slaughter JP, Zhang Z, et al. 2015. A general method to improve fluorophores for live-cell and single-molecule microscopy. *Nat. Methods* 12:244–50
140. Grimm JB, Tkachuk AN, Xie L, Choi H, Mohar B, et al. 2020. A general method to optimize and functionalize red-shifted rhodamine dyes. *Nat. Methods* 17:815–21
141. Los GV, Encell LP, McDougall MG, Hartzell DD, Karassina N, et al. 2008. HaloTag: a novel protein labeling technology for cell imaging and protein analysis. *ACS Chem. Biol.* 3:373–82
142. Gautier A, Juillerat A, Heinis C, Corrêa IR, Kindermann M, et al. 2008. An engineered protein tag for multiprotein labeling in living cells. *Chem. Biol.* 15:128–36
143. Keppler A, Gendreizig S, Gronemeyer T, Pick H, Vogel H, Johnsson K. 2002. A general method for the covalent labeling of fusion proteins with small molecules in vivo. *Nat. Biotechnol.* 21:86–89
144. Gallagher SS, Sable JE, Sheetz MP, Cornish VW. 2009. An in vivo covalent TMP-tag based on proximity-induced reactivity. *ACS Chem. Biol.* 4:547–56
145. Abdelfattah AS, Kawashima T, Singh A, Novak O, Liu H, et al. 2019. Bright and photostable chemigenetic indicators for extended in vivo voltage imaging. *Science* 365:699–704
146. Wang L, Hiblot J, Popp C, Xue L, Johnsson K. 2020. Environmentally sensitive color-shifting fluorophores for bioimaging. *Angew. Chem. Int. Ed.* 59:21880–84
147. Horton NG, Wang K, Kobat D, Clark CG, Wise FW, et al. 2013. In vivo three-photon microscopy of subcortical structures within an intact mouse brain. *Nat. Photon.* 7:205–9
148. Sinefeld D, Xia F, Wang M, Wang T, Wu C, et al. 2022. Three-photon adaptive optics for mouse brain imaging. *Front. Neurosci.* 16:880859
149. Zhao C, Chen S, Zhang L, Zhang D, Wu R, et al. 2023. Miniature three-photon microscopy maximized for scattered fluorescence collection. *Nat. Methods* 20:617–22
150. Nikolaev VO, Bünemann M, Hein L, Hannawacker A, Lohse MJ. 2004. Novel single chain cAMP sensors for receptor-induced signal propagation. *J. Biol. Chem.* 279:37215–18